5,12-Dihydroindolo[3,2-a]carbazole Derivatives-based Water Soluble Photoinitiators for 3D Antibacterial Hydrogels Preparation

Hong Chen, Timur Borjigin, Christophe Regeard, Pu Xiao, Frédéric Dumur, Jacques Lalevée

5,12-Dihydroindolo[3,2-*a*]carbazole Derivatives-based Water Soluble Photoinitiators for 3D Antibacterial Hydrogels Preparation

Hong Chen [1,2], Timur Borjigin [1,2], Christophe Regeard [3], Pu Xiao [4]*, Frédéric Dumur [5]* and Jacques Lalevée [1,2,]*

[1] Université de Haute-Alsace, CNRS, IS2M UMR 7361, F-68100 Mulhouse, France;

[2] Université de Strasbourg, France;

[3] Université Paris-Saclay, CNRS- CEA, Institute for integrative Biology of the Cell (I2BC), 91198 Gif sur Yvette, France;

[4] Research School of Chemistry, Australian National University, Canberra ACT 2601, Australia

[5] Aix Marseille Univ, CNRS, ICR UMR 7273, F-13397 Marseille, France

***** Correspondance: pu.xiao@anu.edu.au (P.X.); frederic.dumur@univ-amu.fr (F.D.); jacques.lalevee@uha.fr (J.L.)

Abstract: Indolo[3,2-*a*]carbazole alkaloids have drawn increasing interest in recent years due to their potential electrical and optical properties. In this work, we synthesized two novel carbazole derivatives using 5,12-dihydroindolo[3,2-*a*]carbazole as the scaffold. Both compounds were extremely soluble in water, with solubility exceeding 7% in weight. More interestingly, introduction of aromatic substituents contributed to drastically reduce the π-stacking ability of carbazole derivatives and presence of the sulfonic acid groups enabled the resulting carbazoles to be remarkably soluble in water so that these carbazoles could be used as especially efficient water-soluble PIs in combination with co-initiators, i.e. triethanolamine and the iodonium salt, respectively, employed as electron donor and acceptor. Surprisingly, multi-component photoinitiating systems based on these synthesized carbazole derivatives could be used for the *in-situ* preparation of hydrogels containing silver nanoparticles *via* laser write procedure with a LED@405 nm as light source and the produced hydrogels exhibited antibacterial effect against Escherichia coli.

Keywords: carbazole, water-soluble photoinitiating system, photopolymerization, metal nanoparticle, antibacterial hydrogel, 3D printing

1. Introduction

Photopolymerization offers several advantages over the traditional thermal initiation techniques. [1-4] Under light irradiation, for example, rapid reactions can occur between a photosensitizer and different additives, even at low temperatures (notably room temperature). Parallel to this, deep curing can only be observed in the irradiated zone, enabling a spatial control of the produced objects. Furthermore, free radical photopolymerization (FRP) can achieve unparalleled spatial and temporal control under mild conditions.[5-7] As an alternative to UV light sources, light emitting diodes (LEDs) can be used as safer, long-living devices enabling to get precise irradiation wavelengths while reducing energy consumption. [8-10] Given the low light intensity of LEDs, it is necessary to develop new photoinitiators (PIs) with higher reactivity than those previously employed.

Hydrogel refers to a gel with the extremely hydrophilic three-dimensional (3D) network structure, in which the modified hydrophilic residues bind the water molecules inside the net, while hydrophobic groups swell with water. Thanks to their high-water absorption and retention, hydrogels are extensively used across a wide range of industries.[11-14] To fabricate three-dimensional (3D) hydrogels *via* photopolymerization techniques, water-soluble PIs, monomers, and water are mixed together to prepare an aqueous formulation, which is then exposed to light source. Numerous benefits come with this approach, including excellent efficiency, safety, environmental protection, and energy savings. [15] However, there are only few commercially available water-soluble PIs at present. For example, the commonly used water-borne photoinitiator 2-hydroxy-4'-(2-hydroxyethyl)-2-methylpropiophenone (I2959) has a low solubility in water (~ 0.47% in weight) and is only sensitive to UV light. [16,17] TPO-Li, another effective and commercial water-soluble PI, has enhanced water solubility over I2959. [18,19] Lithium phenyl-2,4,6-trimethylbenzoylphosphonate (LAP), which is commonly used for the

preparation of biological materials, is a blue light-sensitive photoinitiator with excellent water-solubility. It also exhibits a good biocompatibility and high reaction performance.[20,21] Based on the ongoing increase of the national expenditure for environmental protection, aqueous photopolymerization has been identified as an environmentally friendly approach, and its scope of application can be extended to food packaging materials and biomedical fields.[22] Therefore, the design and synthesis of water soluble PIs has become a new frontier in the research of PIs. Recently, a blue food colorant indigo carmine-based water soluble photoinitiating system has been developed and can efficiently initiate the photopolymerization of poly(ethylene glycol) diacrylate (PEG-DA)-based water-borne formulation under green or blue LED.[23] More interestingly, it was also able to act as both the photoinitiator and the light absorber for the rapid and high-fidelity 3D printing.

Carbazole is an important class of heterocyclic compound that was discovered in 1872 and which is commonly used as a pharmacological precursor due to its numerous biological activities such as antitumor, antiepileptic, antibacterial, anti-inflammatory, antioxidant, and analgesic, etc.[24-29] Moreover, this backbone has also undergone extensive research in the design of Type I or II PIs due to its remarkable electron and charge transport ability, as well as adapted photophysical properties (excited state lifetimes, redox potential) that have efficiently interacted with various additives added to the light-curing resins over the past few decades.[30,31] Several carbazole derivatives have previously been investigated in our group as PIs for polymerization. In these works, different carbazole derivatives exhibited strong optical absorption qualities in the UV/visible wavelength region but also high photoinitiation ability for free radical polymerization.[32-34] However, water solubility was not considered as a priority factor in these different works so that all these carbazoles were totally insoluble in water.

To design water-soluble carbazoles, 5,12-dihydroindolo[3,2-*a*]carbazole has been identified as an interesting scaffold for this purpose and two different carbazole derivatives were prepared (see Figure 1). Notably, sulfonic-acid-terminated side chains were used for the functionalization of the carbazole moieties, providing the water solubility properties to the dye. Parallel to this, nitro is a strong electron accepting group

so its introduction onto 5,12-dihydroindolo[3,2-*a*]carbazole could red-shift the optical spectrum of the resultant carbazole compared to the unsubstituted one. It has to be noticed that the chemistry of 5,12-dihydroindolo[3,2-*a*]carbazole is relatively recent since the first attempts of chemical modifications were reported in 2019. [35] In that work, the symmetric substitution of the two carbazole units was investigated. Recently, our group succeeded to asymmetrically substitute the scaffold of the 5,12-dihydroindolo[3,2-*a*]carbazole by mean of a regioselective nitration. One carbazole unit being substituted by a nitro group, numerous chemical modifications could be carried out onto the second carbazole group. [36-38] Additionally, unlike what is done in the present investigation, water solubility of carbazole derivatives was not examined in these different works. Noticeably, the two carbazole derivatives investigated in this work were remarkably soluble in water with a solubility of more than 7% in weight, even for the nitrated dye. To the best of our knowledge, carbazole 1 and carbazole 2 constitute the first examples of water-soluble carbazoles used as photoinitiators of polymerization. The two carbazole derivatives were incorporated into multi-component photoinitiating systems (PISs) using an iodonium salt (Iod), triethanolamine (TEA) or L-arginine (L-Arg) to induce the FRP of aqueous monomers under the LED irradiation and their initiation abilities was investigated. Parallel to the polymerization, the photo-/electro-chemical properties including absorption characteristics of these two carbazole derivatives were investigated to study the electrical transport routes involved in the deep-curing process. Finally, the proposed PISs can be used to successfully fabricate 3D patterns through the direct laser writing, while it could also photochemically reduce the Ag^+ into AgNPs *in situ*. The produced hydrogels not only exhibited reversible swelling behaviors, but the resulting polymers also effectively resisted against the normal growth of Escherichia coli (E. coli).

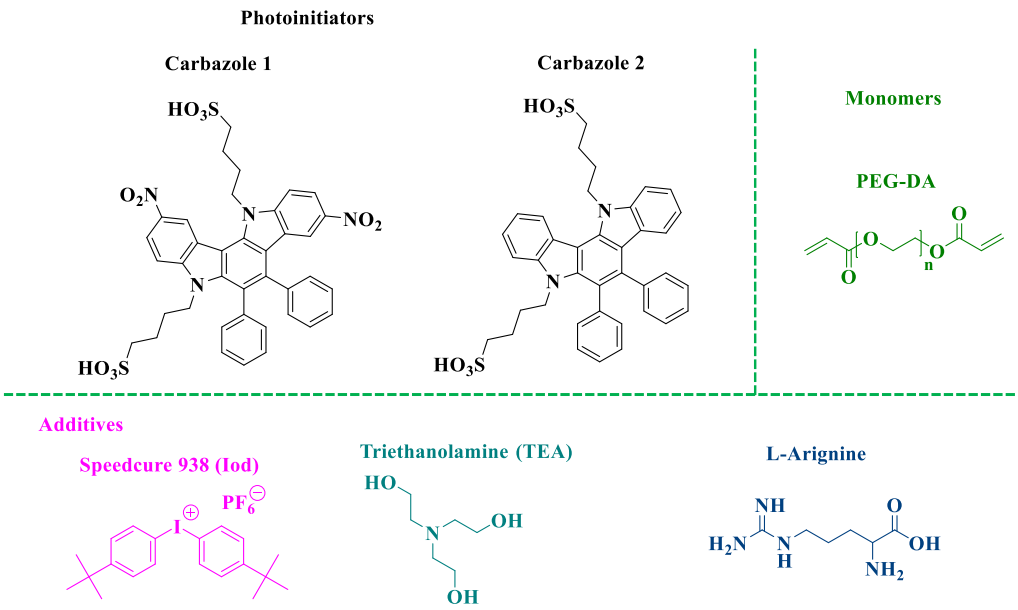

Scheme 1. Chemical structures of the two novel carbazole derivatives, the monomer, and different additives that we used in this study.

2. Experimental Section

2.1. Synthesis of the Two Water-Soluble Carbazole Derivatives

At present, the scaffold of 6,7-diphenyl-5,12-dihydroindolo[3,2-*a*]carbazole has only been scarcely studied in the literature for the creation of carbazoles. The first study on the development of carbazoles employing this scaffold has only been reported in 2019 by Rusinov and coworkers.[35] In this study, only symmetrically substituted derivatives were prepared. More recently, our group investigated in 2022 the possibility to elaborate asymmetrically substituted structures. For this purpose, the nitration of the scaffold of 6,7-diphenyl-5,12-dihydroindolo[3,2-*a*]carbazole proved to be an efficient strategy since a regioselective addition of one nitro group could be selectively obtained, enabling to design Type II photoinitiators.[36,37] To the best of our knowledge, 5,12-dihydroindolo[3,2-*a*]carbazole has never been researched for the purpose of fabricating water-soluble carbazoles, what is investigated in this work. In order to develop mono-component systems, oxime ester derivatives were also prepared as Type I PI with the goal of optimizing the composition of the light-cured formulations.[38,39] However, irrespective of the photoinitiating systems developed (Type I or Type II photoinitiators), no water-soluble dyes were prepared with this structure yet. In the present work, two

structures could be prepared using 1,4-butanesultone as the functionalizing agent for the carbazole units. In fact, choice of sulfonic acid groups as water-soluble agents for our carbazoles was motivated by the unique solubilizing ability sulfonic acid groups exhibit compared to carboxylic acid or phosphonic acid groups.[40] In our case, a subsequent cycloaddition reaction between indole and benzil applying *para*-toluenesulfonic acid as catalyst resulted in the synthesis of a 6,7-diphenyl-5,12-dihydroindolo[3,2-*a*]carbazole core, producing an almost insoluble structure in 77% yield. Then, alkylation of the two carbazole units was carried out in THF using 1,4-butanesultone as the functionalizing agent and providing 4,4'-(6,7-diphenylindolo[3,2-*a*]carbazole-5,12-diyl)*bis*(butane-1-sulfonic acid) in 82% yield. Finally, nitration of 4,4'-(6,7-diphenylindolo[3,2-*a*]carbazole-5,12-diyl)*bis*(butane-1-sulfonic acid) using fuming nitric acid in acetic acid furnished, 4'-(2,9-dinitro-6,7-diphenylindolo[3,2-*a*]carbazole-5,12-diyl)*bis*(butane-1-sulfonic acid) in 90% yield (see **Figure 1**). These two carbazoles, with the exception of DMF and DMSO, were found to be insoluble in ordinary organic solvents. Conversely, upon introduction of the sulfonic groups, the two carbazoles exhibited a remarkable water solubility, despites the polyaromaticity of the structures, evidencing the pertinence of the approach. Besides, it has to be noticed that even if polyaromatic, the two peripheral phenyl rings standing perpendicular to the polycarbazole core efficiently impede the π-stacking of the carbazoles, improving their water solubility. Finally, the proposed carbazoles were then constantly added to water until saturation to examine their solubility.

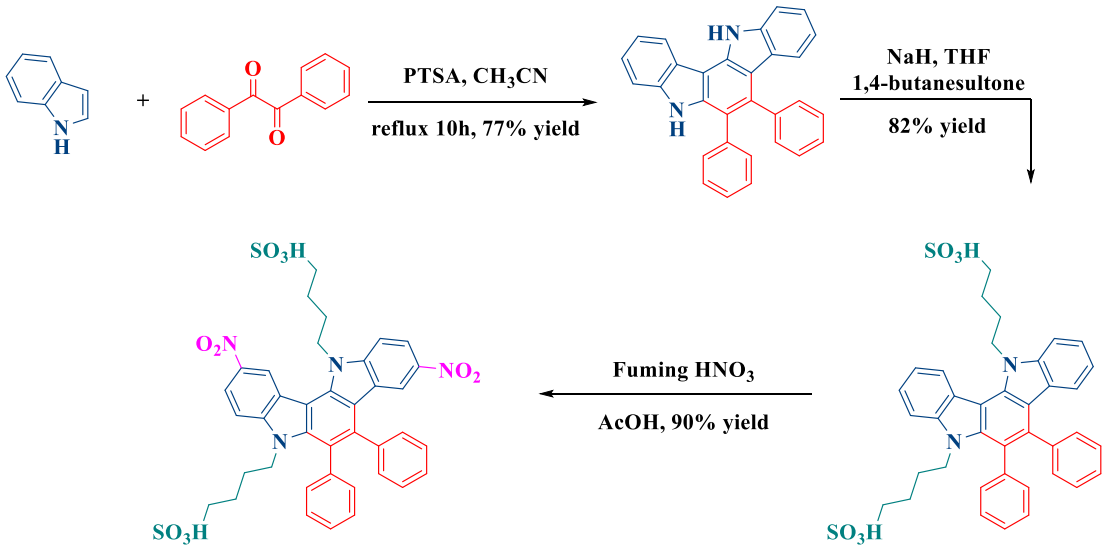

Figure 1. Synthetic routes to the water-soluble two novel carbazole derivatives.

2.2. Other Materials

Triethanolamine (TEA, in Scheme 1) and L-Arginine (L-Arg, see Scheme 1), which serve as co-initiators, the benchmark monomer PEG-DA (M_n = 600 D, see Scheme 1), tetrabutylammonium hexafluorophosphate as supporting electrolytes as well as the other reagents were obtained from domestic suppliers and employed as received. The additive *bis*(4-*tert*-butylphenyl)iodonium hexafluorophosphate (see Scheme 1), abbreviated to Iod, was pruchased from Sartomer-Lambson UK.

2.3. Involved Chemical Mechanisms

UV–Vis Spectroscopy Experiments: The optical absorptive properties of the synthesized two carbazoles in water were determined using a JASCO V730 UV–*Vis* spectrophotometer. Since the Iod only dissolves in organic solvent, while the prepared carbazoles are dispersed only in DMSO solvent, photolysis of the prepared two carbazole derivatives with or without the additives (TEA, Iod) were studied in DMSO under the irradiation of a LED@405 nm, maintaining a concentration of 5×10^{-3} wt% for the proposed carbazoles and 1.5 wt% for the additives (e.g. Iod and amine).[41] Optical absorption spectra were recorded at different exposure intervals.

Fluorescence Spectroscopy Experiments: Fluorescence characteristics of the proposed carbazoles were assessed in water as well as in DMSO solvent using a JASCO

FP-6200 Spectrofluorimeter. Additionally, the fluorescence spectra of the DMSO solution containing the produced carbazoles after the continual addition of additives were recorded in order to analyze the fluorescence quenching induced by interactions of the synthesized carbazoles with Iod or amine. [42]

Cyclic Voltammetry Experiments: The redox potentials (E_{ox}/E_{red}) of the prepared carbazoles were also assessed, and the procedure was performed using cyclic voltammetry, which has been described in detail by us in [34,41]. The free energy change ΔG_{et} for the electron transfer reaction occurring as shown in Scheme 2 was calculated from

$$\mathbf{\Delta G_{et} = E_{ox} - E_{red} - E_S + C}$$

where E_{ox}, E_{red} and E_S stand for redox potentials, and the singlet state energy of the PI (estimated by the carbazoles' optical absorption and fluorescence spectra), respectively. C is typically ignored in polar solvent.[43]

ESR Spin Trapping Experiments: An X-Band spectrometer (Bruker EMX-Plus) was used to study their ESR spectra. In N_2 saturated DMSO solutions, the generation of radicals were triggered exposure to sunlight, and then captured by phenyl-*N*-*tert*-butylnitrone in accordance, the observed spectra were mimicked through detailed procedure. [44]

2.4. Efficiency of Prepared Water-Soluble Carbazole Derivatives for FRP

The functional conversion of aqueous monomer (PEG-DA : water=30%:70%, 50%:50%, 70%:30%, w/w) was followed by RT-FTIR (JASCO FTIR 4700, Lisses, France) to assess the initiating ability of the prepared carbazoles as PIs and carbazoles-based multi-component PISs, like dye-amine (TEA/L-Arg), dye-Iod, dye-Iod-amine, etc. Despite the fact that both additives - TEA and L-Arg – have excellent hydrophilic characteristics, TEA is more easily soluble in aqueous resins than L-Arg. To get a suitable dispersion formulation, Iod must be combined with PEG-DA as the iodonium salt is insoluble in water. In references [34,41], a detailed description of the procedures to analyze the free radical polymerization kinetics of aqueous monomers by RT-FTIR may be found. The final conversion of functional group was calculated from

$$\mathbf{FCs\ (\%) = (1- A_0/A_t)*100}$$

where A_0 and A_t signify the area of functional group's peaks, while the subscripts t and 0 stand for the final irradiation time and the beginning of the curing, respectively.[45]

2.5. Characteristic of the Produced Hydrogel

A Haake-Mars rheometer was also used to investigate the efficiency of FRP of the formulations composed with aqueous monomer (PEG-DA: water=30%:70%, 50%:50%, 70%:30%, w/w). The photopolymerizations process was monitored by tracking the storage modulus of the 20 μL of photocurable formulations exposed to LED @ 405 nm at 25 ºC.

An Instron dynamometer was used to analyze the tensile strength of the produced hydrogels until the hydrogels fractured. At room temperature, at least three measurements were performed for each sample, and the mean values were reported.[46]

The swelling behavior of the prepared hydrogels was investigated following the process described by us in reference [33,40]. The hydrogels' volume increment rate ($\mathbf{V_r}$) and swelling ratio ($\mathbf{S_r}$) were computed utilizing

$$\boldsymbol{S_r}\,(\%) = \mathbf{(W_t - W_0) / W_0*100}$$

$$\boldsymbol{V_r}\,(\%) = \mathbf{V_t / V_0*100}$$

where $\mathbf{W_t}$ **and** $\mathbf{W_0}$ represent the produced hydrogels' wet weight at equilibrium swelling and initial values, respectively; while $\mathbf{V_t}$ **and** $\mathbf{V_0}$ indicate their corresponding volumes.[47]

2.6. Fabrication of AgNPs Encapsulated Hydrogels

Photosensitive formulations were prepared by first mixing the carbazoles/Iod/TEA as PIS (0.1:1.5:1.5 in weight) with aqueous monomer and then adding 2 wt% $AgNO_3$. After that, we were able to fabricate hydrogels with evenly dispersed AgNPs and analyze the influence of photochemical reduction of Ag^+ on the FRP of aqueous monomer by RT-FTIR process as described in 2.4.[48]

2.7. Laser Direct Write Experiments

Using a laser diode @405 nm (Thorlabs, SLA PRINTER), the prepared photocured resins were successfully subjected to direct laser write tests at room temperature, yielding 3D hydrogels. A digital optical microscope (DSX-HRSU from Olympus Corporation) was used to examine the manufactured 3D hydrogels' shape and accuracy.

2.8. Antibacterial Effect of AgNPs Encapsulated Hydrogels

E. coli was employed as a model bacterium to illustrate the antibacterial effect of the manufactured AgNPs-encapsulated hydrogels. The group without hydrogel worked as a blank control, while the group an AgNP-free hydrogel was served as experimental controls. E. coli strains were grown for about 12h in LB medium at 37 °C to establish a new culture until OD_{580nm} = 1 (about 109 bacteria/mL). Then, a new LB agar dish and a new LB liquid medium were also inoculated with 100µL; following overnight growth with AgNP-free hydrogels and AgNPs contained hydrogels, antibacterial activity was then instantly seen by eyes.[49]

3. Results and Discussion

3.1. Solubility of the Prepared Two Carbazole Derivatives In Water

To examine the solubility of the prepared two carbazole derivatives, their concentrations were gradually increased from 0.1 wt% up to 9 wt% in water. As shown in **Figure 2**, they were all easily soluble in water, and the solution of dye 2 progressively darkens from light yellow to yellow, while the dye 1's solution gradually deepens from yellow to brownish yellow. Notably, the solution continued to be transparent even after the concentration of dye 1 was increased to 9 wt%. The aqueous solution, however, became murky when the concentration of dye 2 was raised from 7 wt% to 9 wt%. This result suggested that the dye 1's saturation concentration exceeded 9 wt%, whereas the maximum water solubility of dye 2 may be close to 7 wt%. It was found that introducing the nitro group into the dye caused the darker color and the improved solubility. Interestingly, the solubility of these prepared carbazoles is considerably higher than that of benchmark water-soluble PI (roughly 0.47 wt% for I2959 [16,41]).

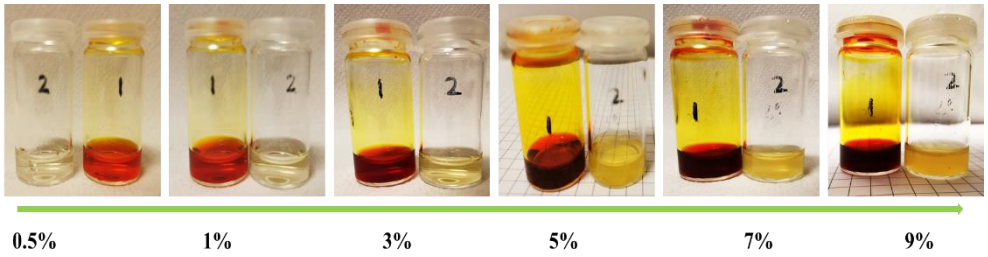

Figure 2. Photographs of the synthesized two carbazole derivatives at concentrations ranging from 0.1 wt% to 9 wt% in water.

3.2. Investigation of the Involved Chemical Mechanisms

The synthesized novel two carbazole derivatives were examined for their light absorption in water, the spectra are depicted in **Figure 3** with the related optical characteristics listed in **Table S1**. It was obvious that carbazole 1 absorbed widely in UV-visible region, with typical absorption maxima at 280nm and 420 nm, which was consistent with the emission spectra of LED@405 nm. In contrast, two optical absorption peaks for dye 2 were detected, respectively, at 290 nm and 370 nm. This indicated that due to the introduction of nitro group to the carbazole's chemical structure, their π-conjugation space was enhanced, resulting in a noticeable red-shift of the absorption and a higher molar extinction coefficient.

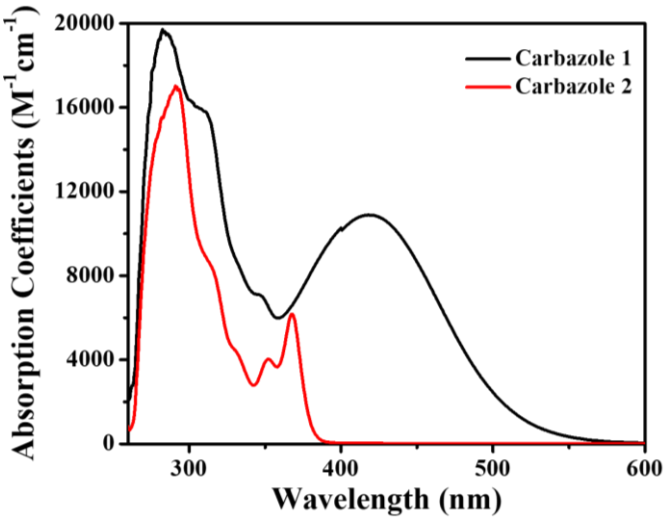

Figure 3. UV-vis absorption spectra of the prepared two carbazole derivatives (carbazole 1 and carbazole 2) in water.

The photolysis process between these two carbazoles and Iod/amine was investigated in DMSO as the solvent since the additives and the proposed two carbazoles were co-soluble in this substance. Under irradiation at 405 nm, as shown in **Figure 4**, essentially no photolysis was observed for the solution of carbazole 1 and carbazole 1-Iod, whereas photolysis process was clearly observed for the solution based on carbazole 1-TEA and the carbazole 1-Iod-TEA, and the absorbance at the characteristic peak around 420 nm steadily decreased with the light irradiation, showing a relatively rapid reaction between carbazole 1 and amine. Even after being exposed to LED@405 nm for 30 min, no substantial photolysis of carbazole 2 was seen (see **Figure S1**), which was consistent with its low absorption properties at the latter wavelength.

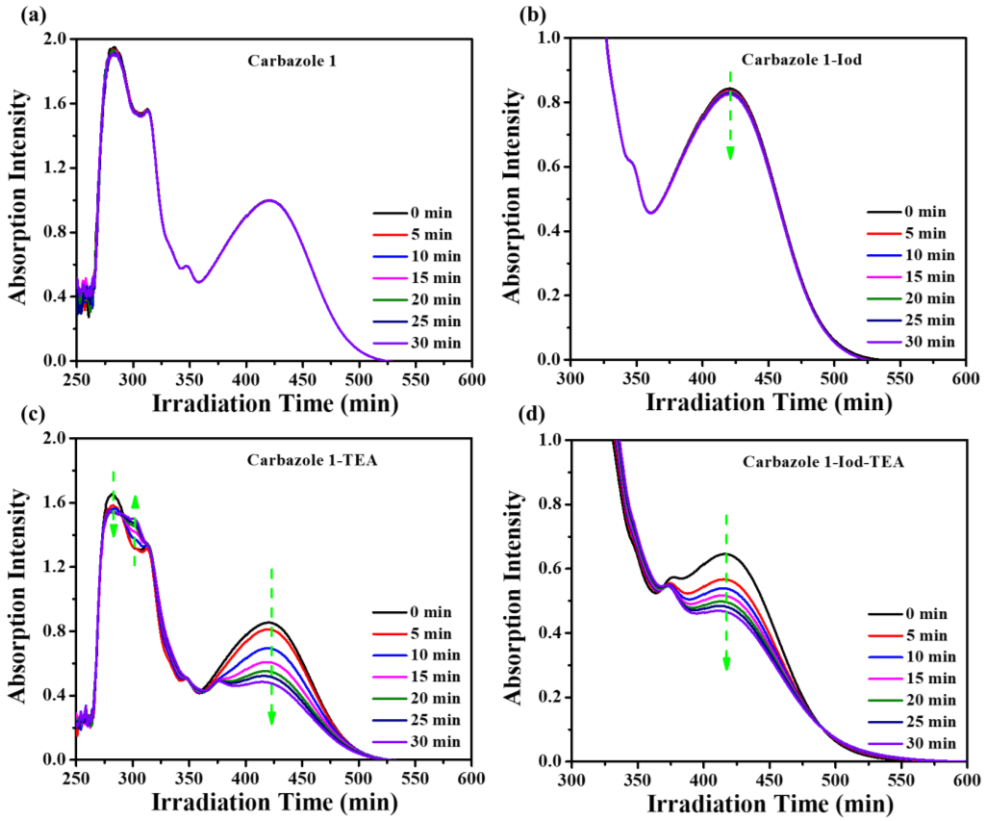

Figure 4. Photolysis of carbazole 1, carbazole 1-Iod, carbazole 1-TEA and carbazole 1-Iod-TEA in DMSO exposed to a LED@405nm.

To further evident the charge transfer reaction occurring between the prepared carbazole derivatives and Iod/TEA, the fluorescence quenching of the proposed carbazoles was explored by adding Iod/amine into the DMSO solution just containing carbazole 1 or carbazole 2. For the solution of carbazole 1, no fluorescence quenching was observed, since their emission intensity did not decrease or even increased with the

addition of Iod/TEA. In contrast, Figure 5 depicted the emission spectrum of carbazole 2, with an emission peak about 400 nm, and a continuous decrease of the emission intensity of the solution of carbazole 2 with the addition of Iod/amine was detected. Notably, as shown in **Figure 5,** the nonlinear curves described the intramolecular quenching processes of carbazole 2-Iod as well as carbazole 2-amine, indicating that collisional quenching was mainly taken place between the carbazoles and additives, meanwhile static quenching may also exist. These findings imply that there was an interaction between carbazole 2 and iodonium/amine.

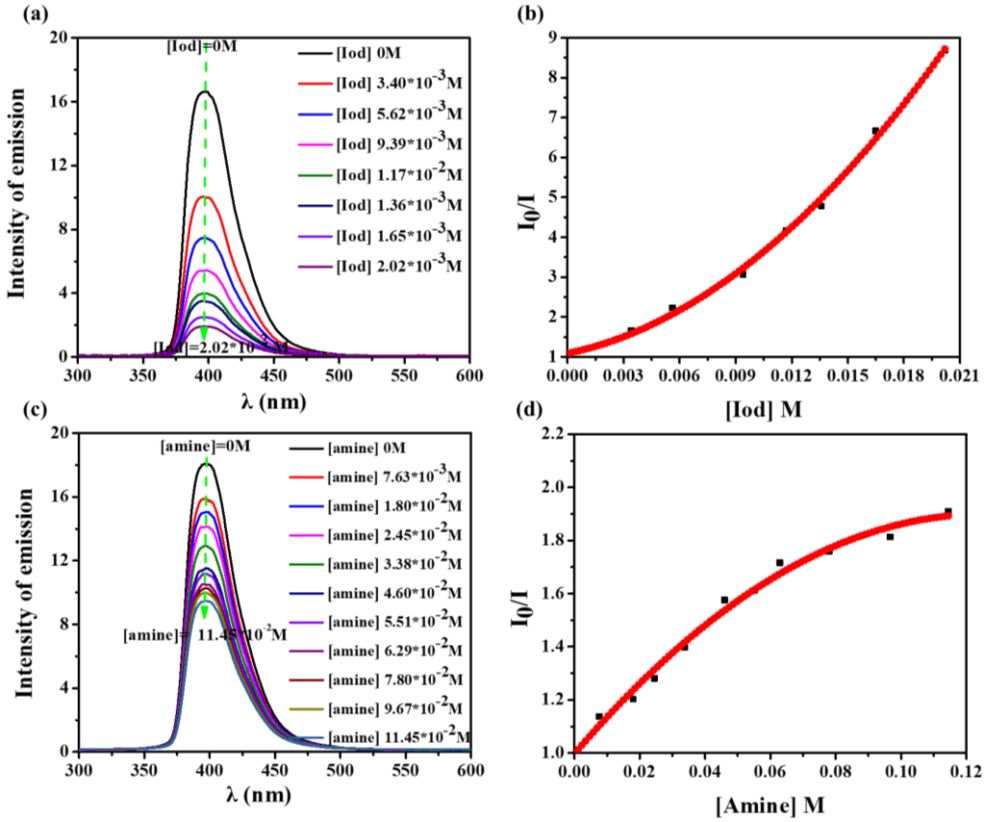

Figure 5. Fluorescence spectra for (a) carbazole 2-Iod solution and (c) carbazole 2-TEA solution during the quenching process; as well as the Stern-Volmer relationship for the intramolecular quenching processes of (b) carbazole 2-Iod and (d) carbazole 2-TEA, respectively.

Based on the above results, we hypothesized the interactions between carbazoles and additives exposed to visible light occur as shown in Scheme 2 and the free energy change (ΔG_{S1}) for the aforementioned reactions were also estimated. First, cyclic voltammetry was used to evaluate the redox potentials of carbazoles 1 and 2 (e.g. E_{red} for carbazole 1: ~-0.41 eV and carbazole 2: ~-0.70 eV). The singlet state energy (E_{S1}) was then explored by normalizing the UV-*Vis* absorption and fluorescence spectra and

working out the crossing point of the two curves (see **Table 1** and **Figure S2**, calculation of E_{S1} for carbazole 1: ~2.60 eV and carbazole 2: ~3.28 eV). Last but not least, based on the previous results, the free energy changes of the interaction (r2 and r3) as shown in **Scheme 2** were calculated to be negative (e.g. carbazole 1 with TEA ΔG_{S1}^{TEA} =-1.19 eV and carbazole 2 with TEA ΔG_{S1}^{TEA} =-1.58 eV), displaying that the above-mentioned interactions as shown in **Scheme 2** can take place under light irradiation.

PBN/Aryl radical (Ar•) adducts were easily identified in ESR-ST tests (see in **Figure S3a**) as Ar• radicals can be generated through the carbazole 2/Iod interaction as shown in r1-2 in **Scheme 2**. Indeed, typical hyperfine coupling constants (hfcs) for PBN/Ar• radical adducts (aN = 14.9 G and aH = 2.6 G) [41,50] were determined by modeling the experimental spectra and confirmed the existence of the reactions (r1-2). The hyperfine nitrogen and hydrogen coupling constants simulated from the experimental spectra of carbazole 2-TEA solution, shown in **Figure S3b**, were 15.0 G and 2.8 G, respectively, confirming the presence of PBN/aminoalkyl radicals. It provided evidence for the occurrence of the reaction (r3) and the formation of the carbazole-H• and $TEA_{(-H)}$• radical necessary for the photoreduction of Ag^+ into AgNPs, and the deep-curing of PEG-DA.

Table 1. Summary of the free energy changes (ΔG_{S1}) of the interactions between the carbazoles and the additives, as well as the singlet state energy (E_{S1}) and reduction potential (E_{red}) of the prepared two carbazole derivatives.

	Carbazole 1	**Carbazole 2**
E_{S1} (eV)	2.60	3.28
E_{red} (V)	-0.41	-0.70
ΔG_{S1}^{TEA} (eV)	-1.19	-1.58

$\Delta G = E_{ox} - E_{red} - E_{S1} + C$ [41]

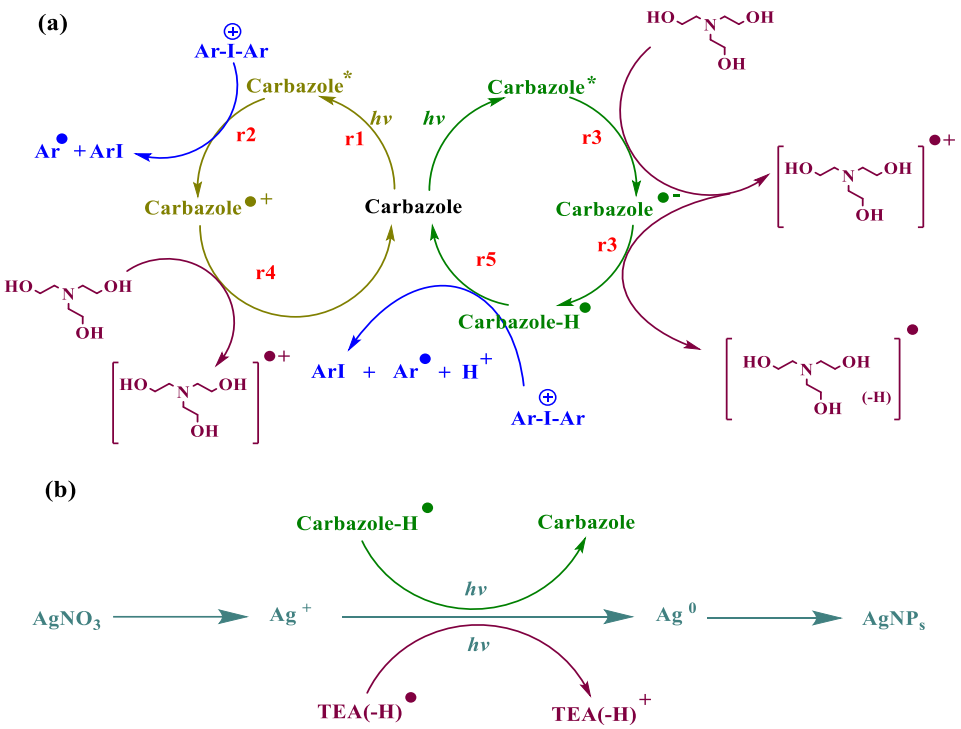

Scheme 2. (a) The photoinitiation mechanisms (r1-r5) of prepared carbazole-Iod-TEA as PIS; (b) the involved photochemical reduction process of the generation of AgNPs.

3.3. Free Radical Photopolymerization Efficiency of the Prepared Carbazole based PISs

Upon expouse to LED@405 nm, photopolymerization efficiency of carbazoles 1 and 2 alone as PIs and carbazoles-Iod, carbazoles-TEA as well as carbazoles -L-Arg as PISs were explored. **Figure S4** depicts the curing curves of the aqueous monomer prepared from 70% PEG-DA + 30% deionized water, where no polymerization was detected in aqueous resins that just contained carbazole 1 or 2 as the PI. Upon addition of additives, the different carbazoles-based two-component PISs became more effcient in FRP processes, and deep curing was observed only in the carbazole 2-Iod based formulation to prepare thin gel sheets with a thickness of almost 0.1 mm. Noticeably, deep curing was also shown in formulations based on carbazole 2-Iod/carbazole 2-TEA for the preparation of thick gel sheets (thickness about 2 mm).

More interestingly, the photoinitiation efficiency of carbazole-Iod-TEA/L-Arg served as three-component PISs (see **Figure 6**) was much higher than that of the carbazoles as PI and carbazoles-based two-component PISs (i.e. the final acrylate function conversion is 99% for carbazole 2-Iod-TEA based system *vs* 87% for carbazole 2-TEA based system, **Table 2 and Table S2**). Subsequently, to further boost

the free-radical photopolymerization efficiency of the three-component PISs, the proportions of PEG-DA and deionized water were adjusted (PEG-DA: water = 30wt%:70wt%, 50 wt%:50 wt%, 70 wt%:30 wt%). Figure 6 shows that the prepared carbazole-based multi-component PIS initiated aqueous resins with 70 wt% PEG-DA and 30 wt% water to get the best polymerization performance, i.e. high functional conversion (approximately 99% for carbazole 2-Iod-TEA/L-Arg, Table 2 in thick films) and high curing speed (slope of the deep-curing curve). When preparing the formulations, the solution was cleared after all compounds were thoroughly dispersed. However, after one hour of sitting, the formulation containing L-Arg became slightly murky, whilst the formulation containing TEA remained clear, indicating that dye-Iod-TEA is the best candidate for application as a water-soluble PIS.

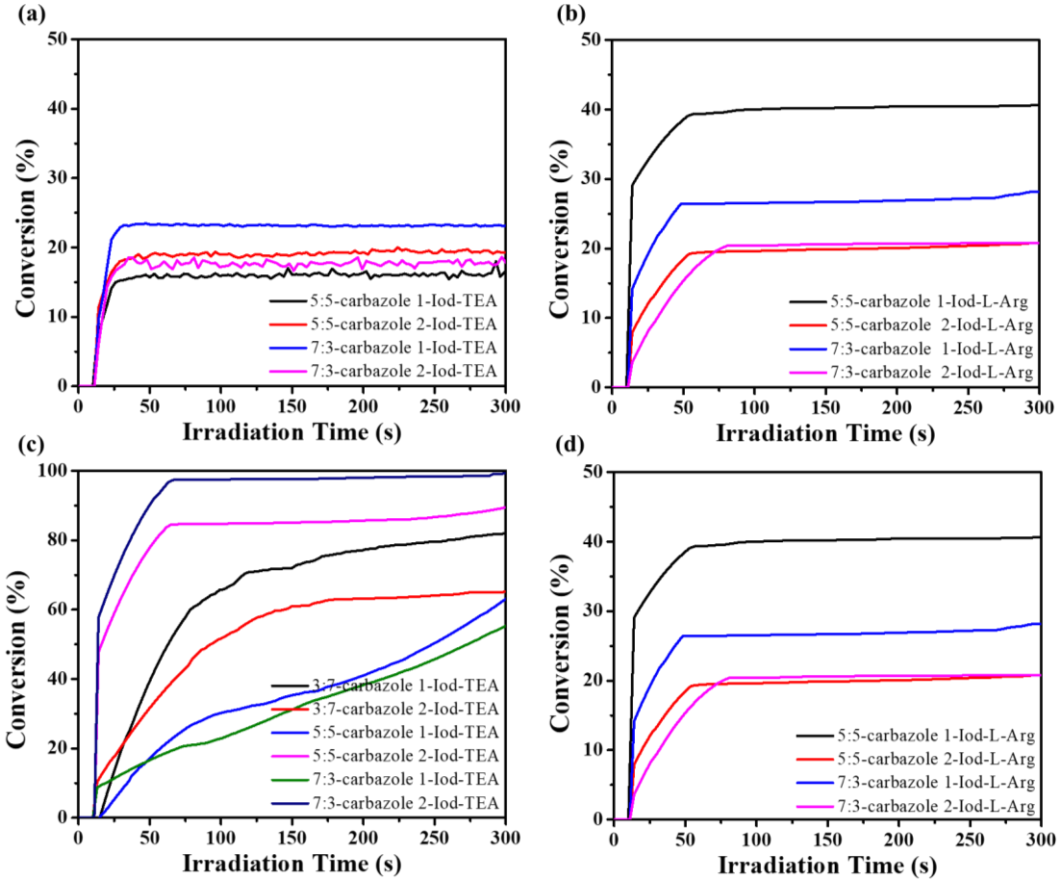

Figure 6. Deep-curing curves (conversion of acrylate groups *vs* time) for the production of hydrogels initiated by carbazole-Iod-TEA and carbazole-Iod-L-Arg as the PIS upon expose to LED@ 405 nm with thickness of (a) almost 0.1 mm and (b) almost 2 mm. The PEG-DA/water contents are 30/70; 50/50 and 70/30 (w/w), respectively: noted 3:7; 5:5 and 7:3, respectively. Irradiation starts at t = 10 s.

Table 2. Summary of the final acrylate function conversions of resins initiated by carbazole-Iod-TEA and carbazole-Iod-L-Arg as PIS exposed to LED @ 405 nm with thickness of almost 0.1 and 2 mm. The PEG-DA/water contents are 30/70; 50/50 and 70/30 (w/w), respectively: noted 3:7; 5:5 and 7/3, respectively.

Final Acrylate Group Conversions				
	Carbazole 1		**Carbazole 2**	
	Thickness ~ 0.1 mm	**Thickness ~ 2 mm**	**Thickness ~ 0.1 mm**	**Thickness ~ 2 mm**
3:7 Carbazole-Iod-TEA	**-**	**82**	**-**	**65**
5:5 Carbazole -Iod-TEA	17	63	19	89
7:3 Carbazole -Iod-TEA	23	55	18	99
3:7 Carbazole -Iod-L-Arg	-	38	-	69
5:5 Carbazole -Iod-L-Arg	40	45	21	75
7:3 Carbazole -Iod-L-Arg	28	82	21	99

"-" implies that photopolymerization cannot be observed

3.4. Manufacturing of Silver Nanoparticles (AgNPs)

Upon expose to LED@405 nm, as shown in **Scheme 2**, the redox reactions between the prepared carbazole derivatives and Iod/TEA occurred, producing some radicals that could be used to initiate the FRP of aqueous resins, while the produced carbazole-H• and $TEA_{(-H)}$• radical may also reduce Ag^+ to AgNPs *in situ*. The efficiency for FRP of aqueous resins decreased significantly after the addition of 2 wt% silver ions, and the final functional conversion decreased to 44%, as shown in the polymerization curves in **Figure S5**, due to the competitive relationship between the FRP of aqueous resins and the photochemical reduction of Ag^+ into AgNPs. In addition, the *in-situ* generated silver nanoparticles in the produced hydrogels were observed to be irregularly shaped by SEM. (**see Figure S6**).

3.5. Mechanical Behavior of Fabricated Hydrogels

A time-sweep Haake-Mars rotating photorheometer was used to assess the storage (G') modulus during the gelation of hydrogel. The resulting curves were displayed in **Figure 7a** and the visible-light irradiation started at t = 20 s. The prepared carbazoles-based PIS exhibited not only higher water solubility than the reference compound

water-soluble PI I2959, but was also suitable for safer and environmentally friendly visible light sources. Furthermore, the resin with 70 wt% PEG-DA:30 wt% water achieved the fastest curing speed, and carbazoles 1 and 2 based three-component PISs were able to complete gelation and reached the maximum storage modulus (G') in less than 100 s.

Moreover, as shown in **Figure 7b** in tensile property tests, the hydrogels fabricated using I2959 as PI attained an elongation strain of 10%, which equated to an ultimate tensile strength of approximately 0.9 MPa. In addition to the hydrogels employed dye 2-Iod-TEA as PIS and 70 wt% PEG-DA:30 wt% water as monomer gelation upon expose to LED@405nm, which reached a maximum elongation of 9% and a fracture potential of 1.2 MPa, the tensile behavior of the hydrogels made from other proposed dye-based PIS with different PEG-DA contents of monomer was lower than that of the reference hydrogels initiated with I2959. This result revealed that 70/30 PEG-DA: water content in weight was the ideal system for the preparation of hydrogels using these water-soluble carbazole-based PIS, i.e., highest photopolymerization efficiency and the best mechanical behavior.

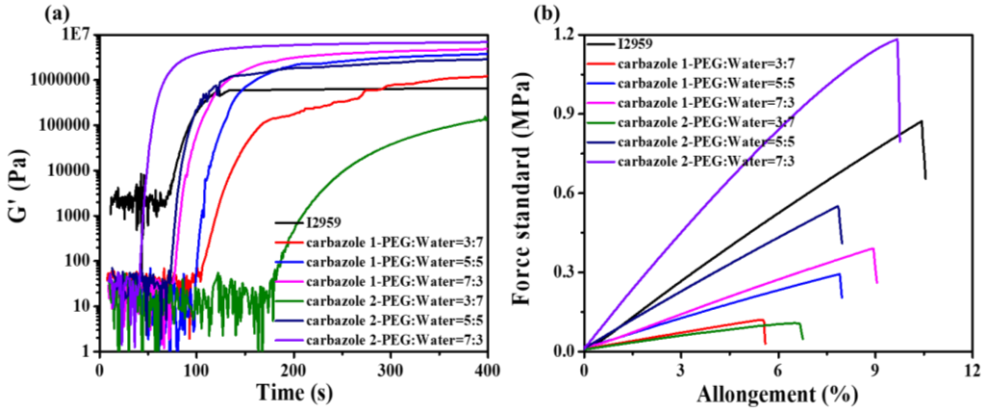

Figure 7. (a) The storage (G′) modulus during the gelation of aqueous resins using I2959 as PI or carbazole-Iod-TEA as PIS; (b) Strain-Stress curves of hydrogels prepared with I2959 and carbazole-Iod-TEA as PIS with/without $AgNO_3$. The PEG-DA/water contents are 30/70; 50/50 and 70/30 (w/w), respectively: noted 3:7; 5:5 and 7/3, respectively.

3.6. Applications in 3D and 4D Printing

As the three-component carbazoles-Iod-TEA system can be employed as effective PIS for the monomers consisting 70 wt% PEG-DA and 30 wt% water exposed to

LED@405nm, laser writing procedures using carbazole 2-Iod-TEA as PIS successfully produced the stable 3D patterns, compared to samples with carbazole 1-Iod-TEA as PIS (1 min for carbazole 2-Iod-TEA as PIS *VS* ~2 min for carbazole 1-Iod-TEA as PIS, see **Figures 8a, 8b**). Furthermore, due to the competition between the photopolymerization process and the photoreduction process, a longer writing time (~5 min, see **Figures 8c, 8d**) was needed to print a 3D pattern after additionally adding 2 wt% $AgNO_3$ to the formulation, and the thickness of the obtained patterns became noticeably thinner. This indicated that the photochemically reduction of Ag^+ limited the polymerization efficiency of aqueous monomer considerably, which was consistent with the results of photopolymerization.

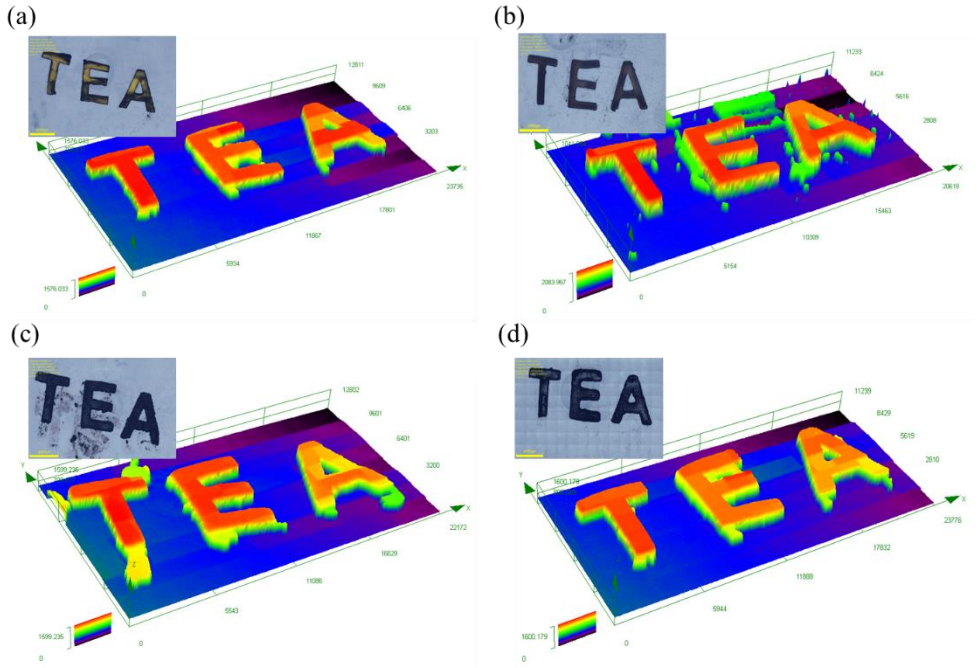

Figure 8. Morphologies of the produced 3D patterns were analyzed by digital optical microscopy: (**a**) prepared using carbazole 1-Iod-TEA as PIS; (**b**) prepared using carbazole 2-Iod-TEA as PIS; (**c**) prepared using carbazole 1-Iod-TEA as PIS after adding 2 wt% $AgNO_3$; (**d**) prepared using carbazole 2-Iod-TEA as PIS after adding 2 wt% $AgNO_3$.

Figure 9 displays the swelling behavior of the four hydrogels produced by the laser writing procedure. The swelling ratio of the hydrogels prepared using carbazoles-based PIS was about 35%. However, after adding $AgNO_3$ into the formulations, the swelling ratio of the hydrogel encapsulating AgNPs decreased significantly as the reduction of Ag^+ and the decrease of hydrophilicity (i.e. the swelling ratio is 35% of

hydrogels *VS* 15% of hydrogels encapsulating AgNPs initiated by carbazole 2-Iod-TEA). It was evident from **Figure S7** and **Table S3** that the structure of the hydrogels and volume increased until reaching swelling equilibrium and then returned to their original or even dry completely after dehydration in an oven.

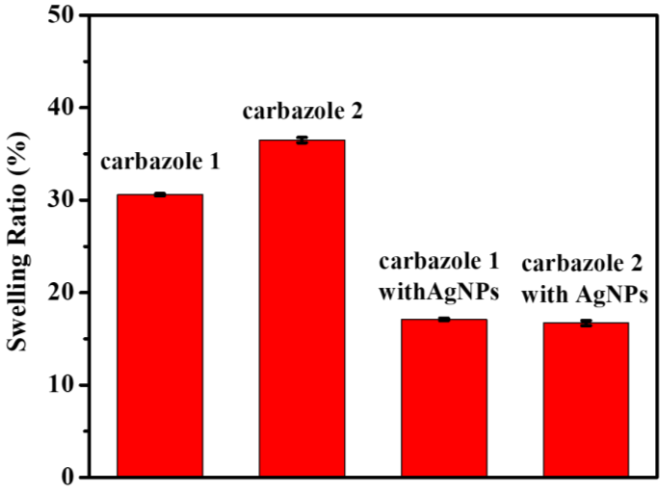

Figure 9. Swelling ratio of pure hydrogels prepared from water-soluble carbazoles 1 and 2 based PISs and hydrogels encapsulated with AgNPs.

3.7. Antibacterial Effect of Prepared Hydrogels

E. coli was employed in this investigation to examine the antibacterial activity of hydrogels encapsulating AgNPs since it was general known that AgNPs have strong antibacterial effects.[51-53] At first, E. coli was cultivated on solid LB-agar utilizing silver nanoparticle-containing hydrogels as the experimental group while pure PEG hydrogels served as the experimental control. After an overnight incubation, it was discovered that a growth inhibition halo was only clearly visible surrounding AgNPs-containing hydrogel (see **Figure 10**). Furthermore, the results by overnight incubation in PBS as shown in **Figure S8** also presented strong antibacterial activity exhibited in the experimental group. Furthermore, in order to determine whether this antibacterial activity was caused by the silver nanoparticles inside the hydrogels, we measured the antibacterial activity of the hydrogels again after soaking them in PBS for 24 h. As depicted in **Figure 10b**, an increase in the area of the growth inhibition halo indicates an enhanced antibacterial activity.

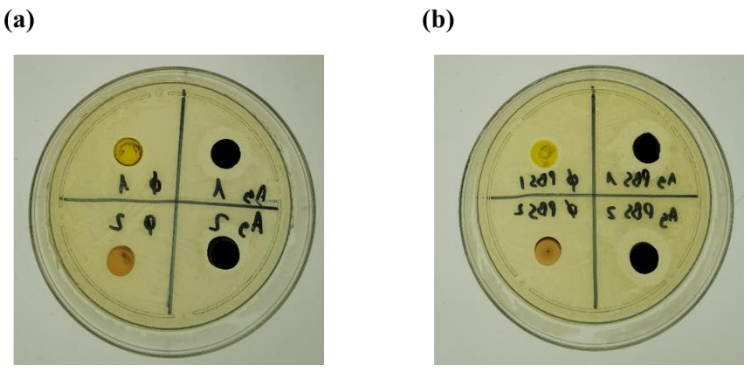

Figure 10. Pictures of Escherichia coli incubated overnight at 37°C with (a) hydrogels without PBS immersion and (b) hydrogels soaked into PBS for 24h. The yellow pieces are pure hydrogels and the black pieces are AgNPs contained hydrogels which initiated by carbazole 1-Iod-TEA as PISs (1) and carbazole 2-Iod-TEA as PISs (2).

4. Conclusions

In this study, two 5,12-dihydroindolo[3,2-*a*]carbazoles were developed and employed as visible light sensitive and water-soluble photoinitiators due to their superior electrochemical and optical qualities, as well as excellent solubility over 70 g/L, resolving the issue of developing effective water-soluble and visible light-sensitive PIs. In addition to achieving a double bond conversion of more than 98% in aqueous resin when combined with additives (Iod/TEA), it also enabled the construction of antibacterial hydrogels containing AgNPs via *in situ* photoreduction of silver ions to silver nanoparticles. Additionally, the proposed PISs were able to successfully produce 3D hydrogel scaffolds that exhibited superior mechanical behavior to those prepared by the commonly used water-soluble photoinitiator I2959 using a SLA printer. Finally, the proposed water-based PISs has shown great potential for the preparation of biosafety photopolymers.

Supplementary Materials: The following Supporting Information is available online. Photolysis of carbazole 2 based PIS; cyclic voltammetry test as well as normalized absorption and emission spectra of two novel carbazoles; ESR-ST spectra of carbazole 2-Iod/carbazole 2-TEA obtained upon expose to sunshine for 5 min; deep-curing curves of the aqueous resin initiated by carbazoles alone as PIs and the carbazoles-based two-component initiating systems upon expose to a LED @ 405 nm; photopolymerization kinetics using carbazole-Iod-TEA based PISs to initiate the FRP of PEG-DA (70 wt%)-

water (30 wt%) containing 2 wt% $AgNO_3$ expose to LED@405 nm; the SEM images of pure PEG-hydrogels and the hydrogels encapsulating AgNPs; Photographs of pure hydrogels and AgNPs encapsulated hydrogels prepared by using dye-Iod-TEA as PIS during the swelling process; pictures of Escherichia coli in 10 ml PBS after incubation overnight at 37°C with the pure PEG-hydrogels and the hydrogels encapsulating AgNPs prepared using dye 2-Iod-TEA as PIS; summary of optical absorption parameters of prepared two novel carbazoles in water; summary of the final acrylate groups conversions of aqueous resins initiated by carbazoles alone as PIs and carbazoles-based two-component PIS; summary the volume of produced hydrogels during the swelling process; the synthesis of two novel 2-indolo[3,2-a] carbazole derivatives.

Funding: This research project is supported by China Scholarship Council (CSC) (201906280059) and the Australian Research Council (FT170100301).

Institutional Review Board Statement: not applicable

Informed Consent Statement: not applicable

Data Availability Statement: No samples available.

Acknowledgments: This research project is supported by China Scholarship Council (CSC) (201906280059). P.X. acknowledges funding from the Australian Research Council (FT170100301).

Conflicts of Interest: The authors declare no conflict of interest.

References:

[1] J. P. Fouassier, J. Lalevée, *Photoinitiators for polymer synthesis: scope, reactivity, and efficiency*, John Wiley & Sons, **2012**.

[2] J. P. Fouassier, *Photoinitiation, photopolymerization, and photocuring: fundamentals and applications.* Hanser, **1995**.

[3] M. D. Nothling, Q. Fu, A. Reyhani, S. Allison-Logan, K. Jung, J. Zhu, G. G. Qiao, *Adv. Sci*. **2020**, *7(20)*, 2001656.

[4] I. Gibson, D. Rosen, B. Stucker, Vat photopolymerization processes. *In. Additive. Manufacturing. Technologies*. Springer, New York, NY. **2015**, 63-106.

[5] J. Li, X. Zhang, J. Nie, X. Zhu, *J. Photoch. Photobio. A.* **2020**, *402*, 112803.

[6] J. Wu, Z. Zhao, C. M. Hamel, X. Mu, X. Kuang, Z. Guo, H. J. Qi, J. Mech. *Phys. Solids.* **2018**, *112*, 25-49.

[7] H. Mokbel, B. Graff, F. Dumur, J. Lalevée, *Macromol. Rapid. Commun*. **2020**, *41(15)*, 2000289.

[8] K. D. Jandt, R. W. Mills, *Dent. Mater.* **2013**, *29(6)*, 605-617.

[9] N. Corrigan, J. Yeow, P. Judzewitsch, J. Xu, C. Boyer, *Angew. Chem. Int. Ed.* **2019**, *58(16)*, 5170-5189.

[10] Y. J. Zhang, Y. Y. Xu, A. Simon-Masseron, J. Lalevée, *Chem. Soc. Rev.* **2021**, *50(6)*, 3824-3841.

[11] E. M. Ahmed, *J. Adv. Res.* **2015**, *6(2)*, 105-121.

[12] T. Huang, H. G. Xu, K. X. Jiao, L. P. Zhu, H. R. Brown, H. L. Wang, *Adv. Mater.* **2007**, *19(12)*, 1622-1626.

[13] A. M. Mathur, S. K. Moorjani, A. B. Scranton, *J. Macromol. Sci. Polym. Rev.* **1996**, *36(2)*, 405-430.

[14] Y. S. Zhang, A. Khademhosseini, *Science*. **2017**, *356 (6337)*, 1-10.

[15] K. T. Nguyen, J. L. West, *Biomaterials*. **2002,** *23(22)*, 4307-4314.

[16] T. N. Eren, N. Kariksiz, G. Demirci, D. Tuncel, N. Okte, H. Y. Acar, D. Avci, *Polym. Chem.* **2021**, *12(18)*, 2772-2785.

[17] B. D. Fairbanks, M. P. Schwartz, C. N. Bowman, K. S. Anseth, *Biomaterials*. **2009**, *30(35)*, 6702-6707.

[18] C. M. Q. Le, L. Vidal, M. Schmutz, A. Chemtob, *Polym. Chem.* **2021***, 12(14)*, 2084-2094.

[19] T. Wiesner, M. Haas, *Dalton. Trans*. **2021**, *50(36)*, 12392-12398.

[20] D. D. McKinnon, A. M. Kloxin, K. S. Anseth, *Biomater. Sci.* **2013**, *1(5)*, 460-469.

[21] B. D. Fairbanks, M. P. Schwartz, C. N. Bowman, K. S. Anseth, *Biomaterials.* **2009**, *30(35)*, 6702-6707.

[22] H. Zhou, S. B. Bhaduri, *Biomaterials. in. Translational. Medicine.* **2019**, 269-289. Academic Press.

[23] D. Zhu, X. Peng, P. Xiao, *Addit. Manuf.* **2022**, *59*, 103154.

[24] P. Wen, Z. Gao, R. Zhang, A. Li, F. Zhang, J. Li, K. Guo, *J. Mater. Chem. C.* **2017**, *5(25)*, 6136-6143.

[25] B. D. Emmanuel, J. Beevi, S. S. Dharan, *J. Pharm. Sci. Res.* **2020**, *12(10)*, 1271-1277.

[26] T. A. Martin, W. G. Jiang, *Anti-cancer. Agents. Med. Chem.* **2010**, *10(1)*, 247-267.

[27] M. Bashir, A. Bano, A. S. Ijaz, B. A. Chaudhary, *Molecules*. **2015**, *20(8)*, 13496-13517.

[28] A. Głuszyńska, *Eur. J. Med. Chem.* **2015**, *94*, 405-426.

[29] S. H. Pattanashetty, K. M. Hosamani, A. K. Shettar, R. Mohammed Shafeeulla, *J. Heterocyclic. Chem.* **2018**, *55(7)*, 1765-1774.

[30] M. Khalid, A. Ali, R. Jawaria, M. A. Asghar, S. Asim, M. U. Khan, M. S. Akram, *RSC. advances*. **2020**, *10(37)*, 22273-22283.

[31] F. Dumur, *Eur. Polym. J.* **2020**, *125*, 109503.

[32] M. Abdallah, D. Magaldi, A. Hijazi, B. Graff, F. Dumur, J. P. Fouassier, J. Lalevée, *J. Polym. Sci. Part A: Polym. Chem.* **2019**, *57(20)*, 2081-2092.

[33] S. H. Liu, H. Chen, Y. J. Zhang, K. Sun, Y. Y. Xu, F. Morlet-Savary, J. Lalevée, *Polymers*. **2020**, *12(6)*, 1394-1409.

[34] H. Chen, G. Noirbent, Y. Zhang, D. Brunel, D. Gigmes, F. Morlet-Savary, J. Lalevée, *Polym. Chem.* **2020**, *11(40)*, 6512-6528.

[35] N.A. Kazin, N.S. Demina, R.A. Irgashev, E.F. Zhilina, G.L. Rusinov, *Tetrahedron.* **2019**, *75(33)*, 4686-4696.

[36] F. Hammoud, A. Hijazi, S. Duval, J. Lalevée, F. Dumur, *Eur. Polym. J.* **2022**, *162*, 110880.

[37] F. Hammoud, A. Hijazi, M. Ibrahim-Ouali, J. Lalevée, F. Dumur, *Eur. Polym. J.* **2022**, *172,* 111218.

[38] F. Hammoud, N. Giacoletto, M. Nechab, B. Graff, A. Hijazi, F. Dumur, J. Lalevée, *Macromol. Mater. Eng.* **2022**, 2200082.

[39] F. Dumur, *Eur. Polym. J.* **2022**, 111330.

[40] B. L. Rivas, E. Pereira, *Macromol. Symp.* **2003**, *193*, 237-250.

[41] H. Chen, L. Pieuchot, P. Xiao, F. Dumur, J. Lalevée, *Polym. Chem.* **2022**, *13(20)*, 2918-2932.

[42] C. R. Bock, T. Meyer, D. G. Whitten, *J. Am. Chem. Soc.* **1974**, *96(14)*, 4710-4712.

[43] D. Rehm, A. Weller, *Isr. J. Chem.* **1970**, *8(2)*, 259-271.

[44] T. Watanabe, M. Yoshida, S. Fujiwara, K. Abe, A. Onoe, M. Hirota, S. Igarashi, *Anal. Chem.* **1982**, *54(14)*, 2470-2474.

[45] P. Bednarczyk, I. Irska, K. Gziut, P. Ossowicz-Rupniewska, *Polymers*. **2021**, *13(11)*, 1718.

[46] J. L. Drury, R. G. Dennis, D. J. Mooney, *Biomaterials*. **2004**, *25(16)*, 3187-3199.

[47] F. Ganji, F. S. Vasheghani, F. E. Vasheghani, *Iran. Polym. J.* **2010**, *19(5)*, 375-398.

[48] H. Chen, C. Regeard, H. Salmi, F. Morlet-Savary, N. Giacoletto, M. Nechab, J. Lalevée, *Eur. Polym. J.* **2022**, *166*, 111042.

[49] W. R. Li, X. B. Xie, Q. S. Shi, H. Y. Zeng, Y. S. Ou-Yang, Y. B. Chen, *Appl. Microbiol. Biotechnol.* **2010**, *85*, 1115-1122.

[50] Y. Qi, H. Li, J. P. Fouassier, J. Lalevée, J. T. Sheridan, *Holography: Advances. And. Modern. Trends. IV.* **2015**, *9508*, 95080I.

[51] F. Ameen, P. Srinivasan, T. Selvankumar, S. Kamala-Kannan, S. Al Nadhari, A. Almansob, M. Govarthanan, *Bioorg. Chem.* **2019**, *88*, 102970.

[52] R. Salomoni, P. Léo, A. F. Montemor, B. G. Rinaldi, M. F. A. Rodrigues, *Nanotechnol. Sci. Appl.* **2017**, *10*, 115.

[53] A. P. Patil, K. H. Kapadnis, S. Elangovan, *Mater. Sci. Res. India*. **2021**, *18(2)*, 143-153.

TOC graphic:

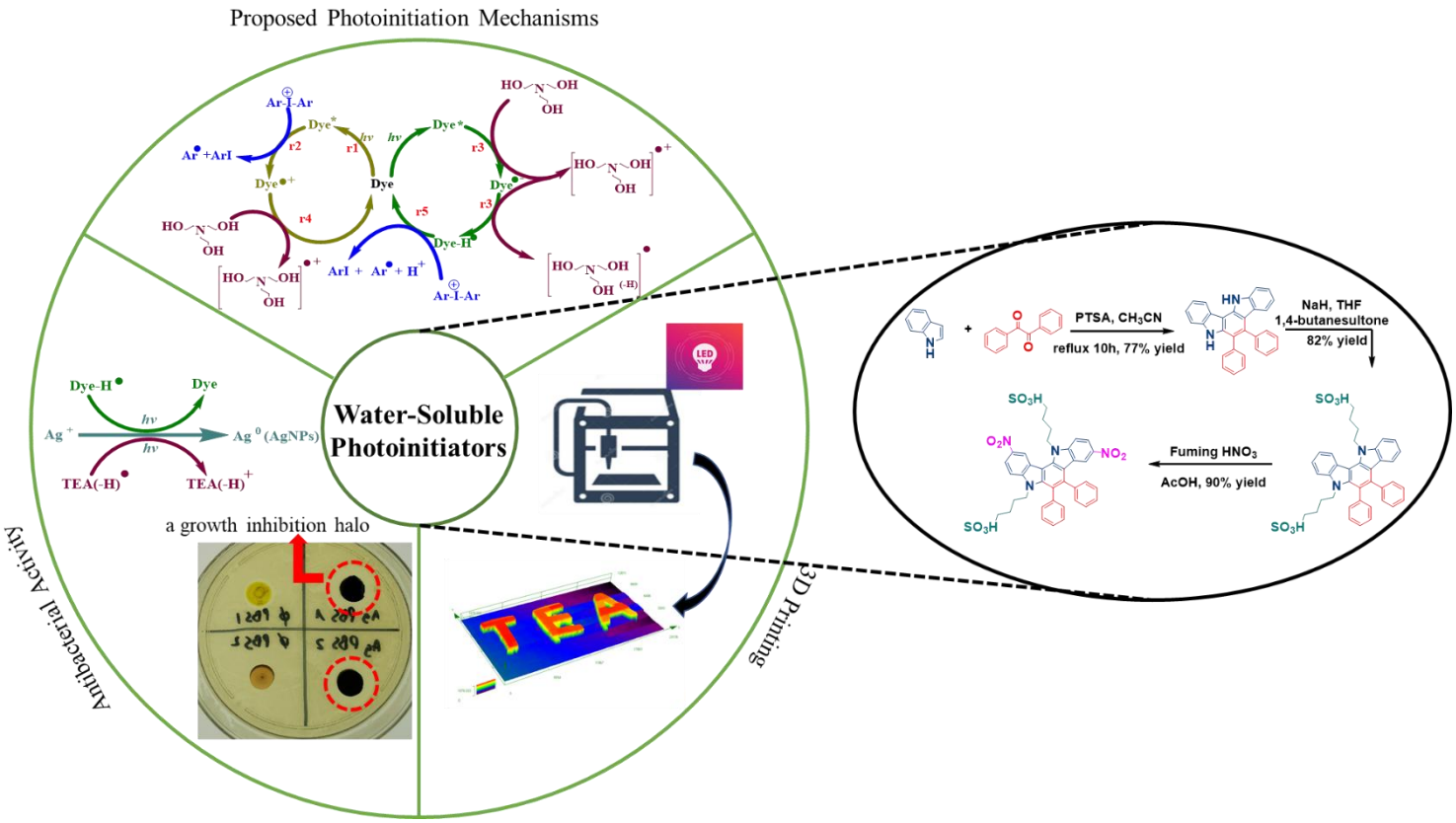
Proposed Photoinitiation Mechanisms
Water-Soluble Photoinitiators
Antibacterial Activity
3D Printing
a growth inhibition halo
PTSA, CH3CN
reflux 10h, 77% yield
NaH, THF
1,4-butanesultone
82% yield
Fuming HNO3
AcOH, 90% yield
TEA